Downloaded from rstb.royalsocietypublishing.org

PHILOSOPHICAL TRANSACTIONS OF THE ROYAL SOCIETY B BIOLOGICAL SCIENCES

Modelling the Pressure and Force Equilibrium in Unipennate Muscles with in-Line Tendons

J. L. Van Leeuwen and C. W. Spoor

Phil. Trans. R. Soc. Lond. B 1993 **342**, 321-333
doi: 10.1098/rstb.1993.0162

Email alerting service Receive free email alerts when new articles cite this article - sign up in the box at the top right-hand corner of the article or click **here**

To subscribe to *Phil. Trans. R. Soc. Lond. B* go to: **http://rstb.royalsocietypublishing.org/subscriptions**

This journal is © 1993 The Royal Society

Downloaded from rstb.royalsocietypublishing.org

Modelling the pressure and force equilibrium in unipennate muscles with in-line tendons

J. L. VAN LEEUWEN[1] AND C. W. SPOOR[2]

[1]*Neuroregulation Group, Department of Physiology, Leiden University, Wassenaarseweg 62, P.O. Box 9604, NL-2300 RC, Leiden, The Netherlands*
[2]*Laboratory for Measurement and Control, Delft University of Technology, Delft, The Netherlands*

CONTENTS

	PAGE
1. Introduction	321
2. Symbols and definitions	322
3. Materials	323
4. The model	323
5. Results and discussion	326
(*a*) Unipennate model with moderate attachment angles of muscle fibres	327
(*b*) Unipennate simulations with large attachment angles of muscle fibres	329
(*c*) Medial gastrocnemius muscle of the cat	329
6. General discussion	331
(*a*) Some determinants of muscle architecture	331
(*b*) Intramuscular pressure and blood flow	332
7. Conclusions	332
References	333

SUMMARY

Several of the models proposed in the literature of unipennate muscles, which have two tendinous sheets and in-line tendons, cannot meet the criterion of mechanical stability. Based on the theory of Van Leeuwen & Spoor (*Phil. Trans. R. Soc. Lond.* B **336**, 275–292 (1992)), we discuss how mechanically stable solutions for (planar) unipennate architectures could be obtained. A mathematical model is proposed in which the muscle architecture is generated numerically using the principles of mechanical stability and assuming that all muscle fibres shorten by the same relative amount. The tendinous sheets are attached tangentially to their respective tendons, as predicted from their low bending stiffness. The curvature, however, is discontinuous at the junction because of the sudden absence of muscle fibres from aponeurosis to tendon. In two of the muscle shapes generated, the sheets adjacent to the tendon show a region of negative curvature connected to a region of positive curvature. A sheet with a concave outer side is defined to have a negative curvature. In another example, two negative curvature regions are present with a positive region in-between. We show also a generated shape with a negative curvature of the sheets over their whole length. A good resemblance was found between the unipennate medial gastrocnemius muscle of the cat and a simulated architecture. The pressure distribution has also been calculated. With all muscle fibres exerting the same tensile stress of 200 kPa, a high pressure region is present in the centre of the muscle belly, half-way along its length. The highest pressures are predicted for muscles with long tendinous sheets, large attachment angles, and strongly curved fibres. Maximum pressures (2.40, 9.54, 10.47, and 7.57 kPa for the four discussed examples, and 15.05 kPa for the simulated gastrocnemius muscle) were at the lower side of the range as predicted previously for bipennate muscles and the unipennate medial gastrocnemius muscle of man (Van Leeuwen & Spoor 1992).

1. INTRODUCTION

The structural elements of skeletal muscle bellies (e.g. tendinous sheets and muscle fibres) have a very low bending stiffness. Mechanical stability, therefore, demands that these structures are curved (Van Leeuwen & Spoor 1992). An intramuscular pressure distribution is generated by curved tendinous sheets

Phil. Trans. R. Soc. Lond. B (1993) **342**, 321–333
Printed in Great Britain

© 1993 The Royal Society

The Royal Society is collaborating with JSTOR to digitize, preserve, and extend access to *Philosophical Transactions: Biological Sciences.* www.jstor.org

Downloaded from rstb.royalsocietypublishing.org

and curved muscle fibres under tension. The concept of stress and pressure equilibrium throughout the muscle belly allows to generate quite realistic muscle shapes as discussed by Van Leeuwen & Spoor (1992). They obtained mechanically stable solutions for muscle architectures by equating the pressure developed by curved muscle fibres with the pressure under a curved tendinous sheet. Muscle geometry was generated numerically using the principle of mechanical equilibrium and the functional demand of equal relative shortening of the muscle fibres. Account was also taken of the space between neighbouring muscle fibres. For reasons of simplicity, Van Leeuwen & Spoor (1992) restricted their analysis mainly to bipennate architectures. They discussed also a unipennate muscle belly which was curved as a whole and compared this architecture to that of the medial head of the human m. gastrocnemius. In this case, the tendon forces at both sides of the muscle are not in line, while mechanical equilibrium is realized through a pressure force at one side of the muscle belly. For this particular case, virtually the same computational scheme could be used as for the bipennate architectures.

By extending the theory by Van Leeuwen & Spoor (1992), we can obtain mechanically stable solutions for unipennate muscles with in-line tendons. This is relevant because unipennate models with in-line tendons have been used by several authors (e.g. Huijing & Woittiez 1984; Woittiez *et al.* 1984; Otten 1985, 1988; Zajac 1989; Spoor *et al.* 1991), whereas none of these models could meet the criterion of mechanical stability (see Van Leeuwen & Spoor 1992). Our aim is to increase the understanding of: (i) muscle shape; (ii) force transmission in the muscle belly; and (iii) the intramuscular pressure distribution. Related and recently reviewed issues as force–length relationships and dynamical aspects of muscles (see Otten 1988; Zajac 1989; Van Leeuwen 1992) will not be discussed.

2. SYMBOLS AND DEFINITIONS

Symbols denoted with ∗ represent normalized quantities.

A_f	total cross-section of all muscle fibres in a muscle belly.
c_f; c_{fc}	curvature of a muscle fibre ($c_f = 1/R_f$); idem, but at the muscle centre, $c_{fc} = 0\ m^{-1}$.
c_s; c_{sc}; c_{sq}	curvature of upper tendinous sheet (allowed to vary along the sheet; $c_s = 1/R_s$); idem, but at the muscle centre; idem, but at $s = q$.
c_t; c_{tc}; c_{tq}	idem, for lower tendinous sheet.
F_f; F_{ft}	muscle-fibre force; part of fibre force transmitted to a particular tendon.
F_{mus}	muscle force.
F_{pc}	internal pressure force exerted on left half of the muscle belly (figure 2*b*).
l_f; l_{fc}	muscle-fibre length; length of muscle fibre at muscle centre.
l_{ts}	total length of the tendinous sheet.
p; p^*	intramuscular pressure; idem, but normalized with respect to the maximum muscle-fibre stress in the muscle belly.
p_c	intramuscular pressure in muscle centre.
p_{max}; p^*_{max}	maximum intramuscular pressure; idem but normalized with respect to the maximum muscle-fibre stress in the muscle belly.
p_{trq}; p_{trlq}	pressure component under the upper tendinous sheet at $s = q$, due to the tensile stress in the tendinous sheet in the transverse direction; corresponding pressure component for lower sheet.
p_q	pressure under upper tendinous sheet at $s = q$.
q	point on upper tendinous sheet.
r_f	co-ordinate in a direction perpendicular to the direction of a muscle fibre.
R_f	radius of curvature of a muscle fibre (assumed to be constant along the fibre).
R_s; R_t	radius of curvature of the upper tendinous sheet (allowed to vary along the sheet); idem, but for the lower sheet.
R_{sq}; R_{tq}	radius of curvature of the upper tendinous sheet at $s = q$; idem, for the corresponding position at the lower sheet.
s	position along upper tendinous sheet (curvilinear co-ordinate).
s_c	length of a tendinous sheet between tip and muscle centre.
T_c	tensile force exerted in each of the tendinous sheets at the muscle centre (figure 2*b*).
T_{sq}; T_{tq}	local tensile force at $s = q$ in the upper tendinous sheet; idem, at corresponding position in lower sheet.
u	exponent in equation (14).
V_f; V^*_f	total fibre volume in muscle belly; volume fraction of muscle fibres with respect to total muscle volume ($V^*_f = V_f/V_{mus}$).
V^*_{floc}	local volume fraction of muscle fibres.
V_{fq}	doubled muscle-fibre volume from $s = 0$ to $s = q$.
V_i; V_{iq}	total interfibre space in muscle belly; doubled interfibre space from $s = 0$ to $s = q$.
V_{mus}	total volume of muscle belly.
V_{tq}	doubled volume from $s = 0$ to $s = q$ (i.e. $V_{fq} + V_{iq}$) (figure 2*d*).
w	width of considered muscle slice, tendinous sheet element or muscle fibre.
α_f; α_{fc}; α_{fq}	attachment angle between lower tendinous sheet and muscle fibre (figure 2*a*); idem, but at muscle centre; idem, but for fibre with $s = q$.
β_f; β_{fc}; β_{fq}	attachment angle between upper tendinous sheet and muscle fibre (figure 2*a*); idem, but at muscle centre (figure 2*a*); idem, but at $s = q$.

Downloaded from rstb.royalsocietypublishing.org

Δr_f thickness of a muscle fibre.
η local fraction at lower sheet to which muscle-fibre tissue is attached.
σ_f; σ_{fc}; σ_{fq} tensile stress exerted by a muscle fibre; idem, but at muscle centre; idem, but at $s = q$.

3. MATERIALS

To check qualitatively our model predictions, we studied the architecture of the medial gastrocnemius muscle of the cat. The architecture of this muscle corresponds closely to the idealized definition of a unipennate muscle with in-line tendons. The attachment at the femur is, however, partly muscular, but more than 95% of the muscle fibres transmit their force via the proximal aponeurosis to the femur. The muscle attaches distally to the calcaneus via the Achilles tendon. Muscles were taken of cats which were used in a research project on neuro-regeneration carried out in the Department of Physiology. The latter project was approved by the local ethical committee. The cats were anaesthetized by an intramuscular dose of Zolethyl (15 mg kg^{-1}, Virbac/Animed, Barneveld, The Netherlands), before they were perfused transcardially with 500 ml lukewarm normal saline, followed by 800 ml citrate buffer (0.1 M; pH 7.1), containing 1.25% glutaraldehyde and 1% paraformaldehyde. Two muscles were completely perfused, whereas two other muscles were only perfused with the saline solution. The latter muscles were studied after they were gone into rigor mortis. All muscles were dissected free by removing the skin and surrounding tissues, while the attachments at the femur and calcaneus were left intact. The muscles were subsequently frozen while being under tension. Thereafter, they were sectioned with a freezing microtome (small tretrander, Jung AG, Heidelberg) so that the central longitudinal plane could be photographed. The pictures were used to make a comparison with a numerically generated muscle shape. A drawing was made of one picture for reproduction in this paper. The pictures themselves were unsuitable for reproduction owing to the low contrast between neighbouring muscle-fibre bundles.

4. THE MODEL

The calculations in this paper apply to a planar unipennate muscle model, with two curved peripheral tendinous sheets and in-line tendons at both sides of the muscle belly. Similar to Van Leeuwen & Spoor (1992) we, in fact, consider the middle longitudinal muscle slice (perpendicular to the tendinous sheets) of width w (w is small compared to the muscle width; see figure 1). This slice is assumed to be in mechanical equilibrium with the neighbouring muscle parts at both sides. The muscle belly depicted in figure 1 was qualitatively discussed by Van Leeuwen & Spoor (1992).

To be able to calculate mechanically stable solutions for unipennate muscle architectures, we make the following simplifying assumptions:

1. The mechanical influence of the connective and adipose tissue surrounding the muscle fibres and fibre bundles is neglected.
2. Each muscle fibre has a constant cross-sectional area, a constant tensile stress, and a constant curvature along its length (these properties are allowed to vary among the muscle fibres). A consequence of the constant curvature assumption (in our two-dimensional approach) is that pressure contours run parallel to the muscle fibres.
3. The very thin layer with tapering muscle fibres under the tendinous sheet (denoted as boundary layer by Van Leeuwen & Spoor 1992) has zero thickness.
4. The tendinous sheets and muscle fibres have no bending stiffness.

Van Leeuwen & Spoor (1992) discussed these assumptions in detail.

In our calculations, we assume that the left and right halves of the muscle belly have identical shapes (the two halves are separated by the central muscle fibre, see figure 2*a*). Therefore, we can limit our calculations to one side of the muscle belly only (we

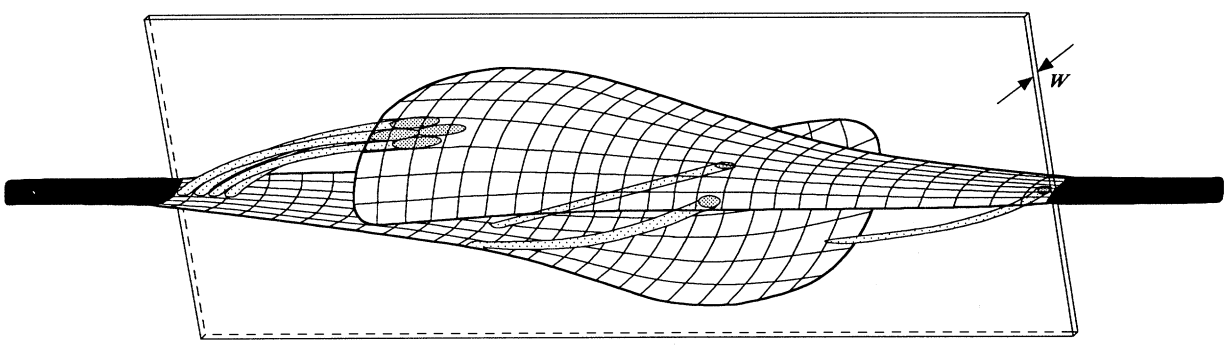

Figure 1. Diagram of a unipennate muscle with in-line tendons (black). The upper tendinous sheet is made transparent for muscle-fibre bundles. Only a few muscle-fibre bundles are shown (stippled). In this paper, we consider quantitatively a slice of width w through the muscle belly. Attachment areas of muscle-fibre bundles are shown also (heavily stippled). A qualitatitve discussion of the three-dimensional mechanical features of this schematized muscle belly was given by Van Leeuwen & Spoor (1992).

Downloaded from rstb.royalsocietypublishing.org

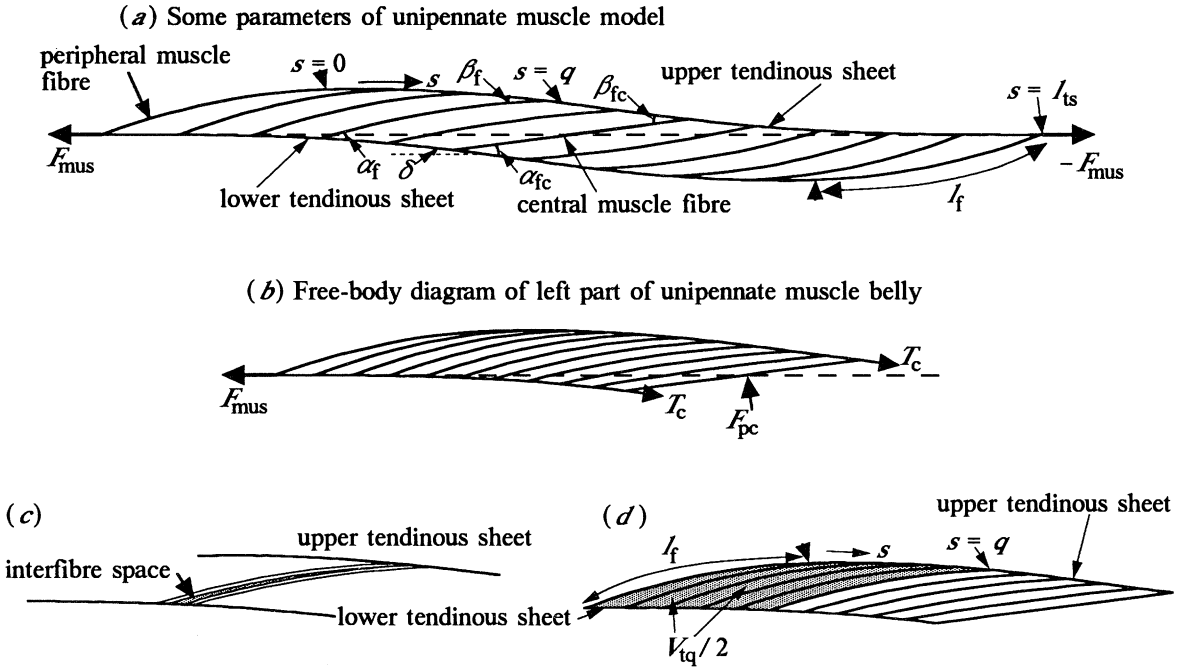

Figure 2. (*a*) Diagram illustrating some parameters of a unipennate muscle model with in-line tendons as explained in the text. Note that the attachment angles of the muscle fibres change by different amounts along the upper and lower tendinous sheets. The dashed line connects the tendons at both sides. (*b*) Free-body diagram of the left part of a muscle belly. (*c*) Illustration of the interfibre space between subsequent muscle fibres of different orientation and curvature. (*d*) The shaded area depicts the volume $V_{tq}/2$. Arrow heads point to the transitions between tendinous sheet and peripheral muscle fibre. See § 2 for symbols.

chose for the left half, see figure 2*b*). However, the model can be easily expanded to asymmetrical bellies. This requires muscle halves to be generated of different shape, but with identical boundary conditions at the muscle centre.

The pressure in the muscle belly is built up along the tendinous sheets by successive layers of curved muscle fibres. We assume that the central muscle fibre is straight, so that the pressure gradient is zero in the centre. Ambient pressure forces are assumed to be negligible. The pressure gradient generated by activated muscle fibres with radius of curvature R_f, curvature c_f ($=1/R_f$), tensile stress σ_f, and thickness Δr_f is given by (Van Leeuwen & Spoor 1992):

$$\partial p/\partial r_f = \sigma_f/R_f = \sigma_f c_f \qquad (1)$$

Let s be a curvilinear co-ordinate describing the distance along the upper tendinous sheet ($s = 0$ at the tip at the left end, $s = s_c$ at the muscle centre, and $s = l_{ts}$ at the point of attachment with the tendon, see figure 2*a*). Let β_f be the attachment angle of a muscle fibre to the upper tendinous sheet, and let α_f be the attachment angle to the lower tendinous sheet. If a muscle fibre is attached over a distance ds onto the upper sheet, then the muscle-fibre thickness is $\sin\beta_f \mathrm{d}s$. For the left muscle half, we assume that no spacing is present between the fibres at their attachments to the upper tendinous sheet. However, spacing between the same fibres is present along their length, and at the attachment to the lower sheet. The situation is reversed for the right muscle half (for reasons of symmetry). Generally, both β_f and α_f vary along the tendinous sheet. The internal pressure generated by the muscle fibres at a point q along s is given by (Van Leeuwen & Spoor 1992):

$$p_q = \int_0^q \sigma_f c_f \sin\beta_f \,\mathrm{d}s = p_c - \int_q^{s_c} \sigma_f c_f \sin\beta_f \,\mathrm{d}s,\ 0 \leqslant q \leqslant s_c, \qquad (2)$$

where p_c is the pressure at the muscle centre.

The pressure under the upper sheet at a point q (figure 2*a*) can be expressed in terms of: (i) the longitudinal tensile force T_{sq} in the tendinous sheet, the local sheet radius of curvature R_{sq} (both T_{sq} and R_{sq} vary along the sheet), and the width w of the slice through the sheet; (ii) a similar term in the transverse direction; and (iii) the local muscle-fibre stress σ_{fq} and the local attachment angle β_{fq} (Van Leeuwen & Spoor 1992):

$$p_q = \frac{T_{sq}}{R_{sq} w} + p_{trq} + \sigma_{fq} \sin^2\beta_{fq}, \qquad 0 \leqslant q \leqslant s_c. \qquad (3)$$

The tensile force (along s) at position q in the upper tendinous sheet can be calculated from the muscle-fibre stress along the sheet and the attachment angle β_f along the sheet (Van Leeuwen & Spoor 1992):

$$T_{sq} = w \int_0^q \sigma_f \cos\beta_f \sin\beta_f \,\mathrm{d}s$$

$$= T_c - w \int_q^{s_c} \sigma_f \cos\beta_f \sin\beta_f \,\mathrm{d}s, \qquad 0 \leqslant q \leqslant s_c, \qquad (4)$$

where T_c, the tensile force in each of the tendinous sheets at the muscle centre, is calculated as:

$$T_c = w \int_0^{s_c} \sigma_f \cos\beta_f \sin\beta_f \,\mathrm{d}s. \qquad (5)$$

Downloaded from rstb.royalsocietypublishing.org

Using equation (4), equation (3) can be rewritten as:

$$p_q = \int_0^q \sigma_f \cos\beta_f \sin\beta_f \, ds/R_{sq} + p_{trq} + \sigma_{fq} \sin^2\beta_{fq}, \quad 0 \leqslant q \leqslant s_c. \quad (6)$$

Now, the muscle pressure p_c at the muscle centre can be derived from the local values of the tensile force in the tendinous sheet per unit width, the sheet curvature c_{sc}, and the muscle-fibre stress σ_{fc}, once the attachment angle β_f and tensile stress σ_f of the muscle fibres as well as the length s_c of the upper tendinous sheet at the left-hand side from the muscle centre are prescribed (see below and figure 2*a*). It is assumed that p_{trq} is either known, prescribed or neglected.

At every position along the upper tendinous sheet in the left muscle half, the pressure generated by the muscle fibres (equation 2) should be equal to the pressure calculated from the tendinous-sheet curvature and tensile force, and the muscle-fibre stress (equation 6). Hence (Van Leeuwen & Spoor 1992):

$$\int_0^q \sigma_f c_f \sin\beta_f \, ds = \int_0^q \sigma_f \cos\beta_f \sin\beta_f \, ds/R_{sq} + p_{trq} + \sigma_{fq} \sin^2\beta_{fq}, \quad 0 \leqslant q \leqslant s_c. \quad (7a)$$

The local radius of curvature of the upper tendinous sheet is obtained by rearranging equation (7a):

$$R_{sq} = \frac{\int_0^q \sigma_f \cos\beta_f \sin\beta_f \, ds}{\int_0^q \sigma_f c_f \sin\beta_f \, ds - p_{trq} - \sigma_{fq} \sin^2\beta_{fq}}, \quad 0 \leqslant q \leqslant s_c. \quad (7b)$$

Equation (7) shows how the upper tendinous sheet shape (left from the muscle centre) can be calculated such that it is compatible with the pressure built up by successive layers of curved and activated muscle fibres. For reasons of symmetry, this shape is equal to the shape of the lower tendinous sheet at the right side of the muscle centre.

We now need to know how the shape of the lower tendinous sheet at the left-hand side from the centre can be calculated. Since the pressure contours are assumed to run along the muscle fibres (see above), the pressure under both tendinous sheets is equal at the two opposite attachments of each particular muscle fibre. Similar to equation (3), we can write:

$$p_q = T_{tq}/(R_{tq} w) + p_{trlq} + \sigma_{fq} \eta \sin^2\alpha_{fq}, \quad 0 \leqslant q \leqslant s_c, \quad (8)$$

where η is the local fraction of the lower aponeurosis to which muscle fibre tissue is attached. This correction term is needed because interfibre spaces are present near the lower sheet. The other parameters correspond to those for the upper sheet in equation (3). The required tensile force in the lower sheet (corresponding to position q at the upper sheet) can be calculated as

$$T_{tq} = T_c + w \int_q^{s_c} \sigma_f \cos\alpha_f \sin\beta_f \, ds = F_{mus} - w \int_0^q \sigma_f \cos\alpha_f \sin\beta_f \, ds, \quad 0 \leqslant q \leqslant s_c, \quad (9)$$

where F_{mus} is the total muscle force (figure 2). For convenience, parameter s is used as integrand here because, along the lower sheet, an a priori unknown amount of interfibre tissue is assumed to be present between the muscle fibres (see below and figure 2*c*). For a particular muscle fibre, s has the same value at both tendinous sheets. Similar to the calculation for the upper-sheet curvature, the curvature of the lower tendinous sheet follows now from formulae (2), (8), and (9):

$$R_{tq} = \frac{\frac{T_c}{w} + \int_q^{s_c} \sigma_f \cos\alpha_f \sin\beta_f \, ds}{\int_0^q \sigma_f c_f \sin\beta_f \, ds - p_{trlq} - \sigma_{fq}\eta \sin^2\alpha_{fq}}, \quad 0 \leqslant q \leqslant s_c. \quad (10)$$

It may be noted that, by introduction of η, we neglect small-scale variations in sheet curvature due to alternating fibres and inter-fibre spaces.

The total muscle force (figure 2) can be calculated from:

$$F_{mus} = w \int_0^{s_c} \sigma_f \cos\beta_f \sin\beta_f \, ds + w \int_0^{s_c} \sigma_f \cos\alpha_f \sin\beta_f \, ds. \quad (11)$$

The first term represents T_c, the force built up from the tip of the sheet to the muscle centre. The second term denotes the force built up from the muscle centre to the point of attachment with the tendon.

A single muscle fibre mostly attaches with different angles on the upper and lower tendinous sheets (or, better, penetrates the boundary layers at different angles). This has consequences for the force transmission of the muscle fibres. The conventional rule that the force transmission to the aponeurosis equals fibre force times the cosine of the attachment angle can be applied to both the upper and the lower aponeurosis. The muscle-fibre force F_f is transmitted to the lower aponeurosis with component $F_f \cos\alpha_f$, and with component $F_f \cos\beta_f$ to the upper aponeurosis. Since β_f deviates from α_f for most of the fibres (the central muscle fibre has equal attachment angles), the forces transmitted to both sheets are different, although the tendon forces have the same amplitude at both sides of the muscle belly (the forces in the longitudinal direction cancel, see free-body diagram of figure 2*a*). For the considered symmetric case, each muscle fibre in one muscle half has a corresponding fibre in the other half with exactly opposite effects on the force transmission. In general, the situation is more complex.

Van Leeuwen & Spoor (1992) defined the effective pennation angle γ_f of a muscle fibre in relation to the transmission of fibre force to muscle-belly force:

$$\gamma_f = \arccos(F_{ft}/F_f), \quad (12)$$

where F_{ft} is the part of the fibre force being eventually contributed to the muscle force. This definition cannot be applied unambiguously to single muscle fibres of the unipennate muscle belly with in-line tendons. Although it was not explicitly stated (Van Leeuwen & Spoor 1992), the forces of single fibres transmitted to both tendons in bipennate architectures are,

PHILOSOPHICAL TRANSACTIONS OF THE ROYAL SOCIETY B BIOLOGICAL SCIENCES
PHILOSOPHICAL TRANSACTIONS OF THE ROYAL SOCIETY B BIOLOGICAL SCIENCES

Downloaded from rstb.royalsocietypublishing.org

in general, also different (therefore, the choice of α_f for γ_f was too simple).

The above set of equations allows to generate numerically a wide range of mechanically stable muscle architectures. Only a subset of this range is expected to correspond to architectures found in nature. To limit the possible variations, we prescribe the length of the muscle fibres in the muscle belly:

$$l_f = l_{fc} \frac{\cos((\beta_f + \alpha_f)/2)}{\cos\beta_{fc}}, \qquad (13)$$

where $\beta_{fc} = \alpha_{fc}$ is the attachment angle at the muscle centre (figure 2*a*) and l_{fc} is the central muscle-fibre length. This choice is loosely based on the assumption that, in an infinitesimal muscle shortening, all muscle fibres should contract by the same relative amount so that work by them is produced in proportion to fibre volume (see Van Leeuwen & Spoor (1992) for a more detailed discussion). Formula (13) leads to an almost constant fibre length throughout the muscle belly (see figure 3*e*).

The attachment angle β_f was (tentatively) described as a power function of s:

$$\beta_f = \beta_{fc}\{s/s_c\}^u, \qquad 0 \leqslant s \leqslant s_c. \qquad (14)$$

The attachment angles along the lower tendinous-sheet part between muscle centre and tendon attachment are calculated during the numerical procedure (see below). Thus, they are not defined a priori.

Now, the volume distribution of muscle fibres and interfibre space within the muscle belly will be considered. The volume of the muscle fibres from two corresponding regions in the two muscle halves is given by:

$$V_{fq} = 2w \int_0^q l_f \sin\beta_f \, ds. \qquad (15)$$

Neighbouring muscle fibres in the muscle belly have slightly different radii of curvature, different attachment angles, while also the sheet orientation differs slightly. Therefore, some space is present between the fibres (figure 2*c*). In calculating this space, it is assumed that the fibres have no space in-between at the attachments from the tip of the sheet to the muscle centre. The interfibre space may be filled with connective tissue, adipose tissue, blood vessels or nerves. In reality, muscle fibres in a slice parallel to the central muscle slice may penetrate the interfibre space of an adjacent slice (Van Leeuwen & Spoor 1992; see also figure 1). Such arrangement has a positive effect on the packing of the muscle fibres. The interfibre space V_{iq} associated with the attached fibres from $s = 0$ till $s = q$ (summed for both muscle halves) can be obtained by subtracting V_{fq} from the total volume V_{tq} of both halves (figure 2*d*) enclosed by the superficial muscle fibre, the upper tendinous sheet up to q, the muscle fibre at q, and the lower tendinous sheet:

$$V_{iq} = V_{tq} - V_{fq}. \qquad (16)$$

Let V_f be the total muscle-fibre volume and let V_{mus} be the total volume of the muscle belly. Then, the global fractional fibre space V_f^* is calculated as V_f/V_{mus}. A local volume fraction of the fibres (V_{floc}^*) was calculated as half the volume of two neighbouring fibres divided by this same volume plus the enclosed interfibre volume.

Summarizing, to calculate the shape of a mechanically stable slice of a unipennate muscle belly, the following strategy was applied:

1. Prescribe the attachment angle along the upper sheet $\beta_f(s)$ from $s = 0$ to $s = s_c$ using equation (14) and prescribe the tensile stress distribution in the muscle fibres.
2. For simplicity, the left half of the muscle belly is 'mathematically clamped' at the muscle centre (figure 2*b*). The clamping (boundary) conditions are prescribed (i.e. tendinous sheet curvature, and muscle fibre attachment angle and length). The central muscle fibre is assumed to be straight. Calculations are made for half a muscle belly only as it is assumed that both halves have identical shapes and corresponding muscle fibres exert equal forces.
3. Initially, give a rough estimate of s_c (the length of the upper tendinous sheet from its free end to the muscle centre). Adjust this length in subsequent iterations so as to converge to the required solution.
4. Starting from the clamping side, calculate (i) the curvature $c_f(s)$ for successive muscle fibres such that the fibre length meets the length criterion of equation (13) (if this would result in overlap of muscle fibres, the nearest fibre curvature and length without overlap is taken), (ii) the corresponding tendinous sheet curvatures R_s and R_t using equations (7) and (10), and (iii) the attachment angle α_f.
5. Step (4) is stopped and the process restarted at step (3) if either the gradient in muscle-fibre curvature falls below or above certain limits, fibres would have to penetrate each other, or the calculated pressure is not close enough to zero at the peripheral muscle fibre boundary. If, however, none of these (ill) conditions are met, then the calculated architecture is accepted as a mechanically stable solution.
6. Calculate the total tendinous sheet length, muscle force, muscle volume, fibre volume, interfibre volume, and volume fractions.

With the prescribed attachment angles and fibre lengths, a unique solution corresponds to a particular set of clamping conditions.

The above model was implemented in a computer programme, allowing to simulate force and pressure development by unipennate muscle bellies.

5. RESULTS AND DISCUSSION

The present model covers an infinite set of solutions for mechanically stable unipennate muscle architectures. Here, we will discuss a few examples only. For simplicity, equal tensile stresses of 200 kPa for all muscle fibres will be used in all simulations in this paper.

PHILOSOPHICAL TRANSACTIONS OF THE ROYAL SOCIETY B BIOLOGICAL SCIENCES
PHILOSOPHICAL TRANSACTIONS OF THE ROYAL SOCIETY B BIOLOGICAL SCIENCES

Downloaded from rstb.royalsocietypublishing.org

Table 1. *Values of input and output parameters of figures 3, 4, and 5*

(The tensile stress of the muscle fibres (σ_f) was set to 200 kPa for all muscle fibres in all simulations. Furthermore, the muscle-fibre length at the muscle centre was chosen to be 10 mm (except in figure 5 where it was set to 21.53 mm). The transverse tensile stress in the tendinous sheets was neglected in all simulations. Other parameter values (per unit width where applicable) are given below.)

		figure numbers				
symbol	unit	3	4*a*,*b*	4*c*	4*d*	5*b*,*c*
input						
c_{sc}	m^{-1}	− 4.651	− 9.091	− 5.587	− 24.272	− 11.112
β_{fc}	°	7.5	15.0	15.0	15.0	20.5
u		1.1	1.1	0.7	0.7	1.4
output						
V_{mus}	mm^2	47.12	93.08	100.05	58.00	476.10
V_f^*		0.462	0.464	0.532	0.420	0.397
A_f	mm	2.175	4.318	5.331	2.448	8.788
s_c	mm	17.47	17.42	17.42	8.00	29.77
l_{ts}	mm	34.90	34.70	34.34	14.73	58.72
F_{mus}	(mN mm^{-1})	430.6	829.7	1024.2	466.6	1621.5
T_c	(mN mm^{-1})	216.6	424.6	523.1	240.2	853.1
p_{max}	kPa	2.40	9.54	10.47	7.57	15.05
p_{max}^*		0.0120	0.0477	0.0524	0.0378	0.0753

(*a*) *Unipennate model with moderate attachment angles of muscle fibres*

(i) *Starting conditions*

In most muscles at optimum length for force output, attachment angles of the muscle fibres are below 25° (cf. Spoor *et al.* 1991; Wickiewicz *et al.* 1983). Figure 3 illustrates the results of a simulation of a unipennate muscle model with moderate angles of attachment of the muscle fibres (parameter values are given in table 1). The chosen value of only 7.5° for β_f at the muscle centre can already be considered as moderate, especially as it is accompanied with a maximum attachment angle of almost 12.5°. The influence of the transverse tensile stress in the tendinous sheets was neglected (i.e. $p_{trq} = p_{trlq} = 0$ in equations 3, 6, 7, 8, and 10).

(ii) *Muscle-fibre arrangement*

Figure 3*a* shows how the muscle fibres are arranged in the muscle belly. In the left half of the muscle belly, α_f is larger than β_f owing to fibre curvature and particular orientations of the tendinous sheets (figures 3*c*,*d*). This leads to a concentration of interfibre space in the muscle belly close to the two tendons (figure 3*e*). The calculated total volume fraction of the muscle fibres is only about 0.46 for this particular architecture. This unrealistically low value is a direct consequence of the two-dimensional approach. Van Leeuwen & Spoor (1992) discussed how, in a real muscle, this problem may be solved by penetration of muscle fibres from the lateral sides into the interfibre spaces. Figure 3*e* shows that the local muscle-fibre fraction increases from about 0 at the tip (left side) of the peripheral tendinous sheet to about 0.86 in the muscle centre. Muscle-fibre length varies only slightly along the muscle belly (figure 3*e*), with the minimum found at the muscle centre. The ideal muscle-fibre length is everywhere equal to the calculated fibre length. The maximum fibre curvature is about 21 m^{-1}.

(iii) *The tendinous sheets*

The curvature of the tendinous sheets has a value of about 12 m^{-1} at the tip, drops to the (prescribed) value of − 4.6 m^{-1} at the muscle centre (the global minimum), has a local maximum of − 4.18 m^{-1} at $s \approx 20.3$ mm and a local minimum of − 4.20 m^{-1} at $s \approx 20.6$ mm, and attaches to the tendon with a curvature of only − 0.02 m^{-1} (figure 3*c*). Owing to the limited graphical resolution, not all details can be seen in figure 3*c*. The tendinous sheets attach tangent to their respective tendons, as expected from their low bending stiffness. The curvature, however, is discontinuous at the junction. This is explained by the sudden absence of attaching muscle fibres from aponeurosis to tendon. The last pressure term of equation (8) vanishes suddenly from aponeurosis to tendon. A jump in the pressure from ambient to the muscle belly can only be avoided if the jump in the last pressure term is compensated by a counteracting jump in the first term (the second term was neglected in the simulations), requiring a negative sheet curvature at the junction.

(iv) *Intramuscular pressure*

The maximum pressure, located at the centre of the muscle, is 2.40 kPa. Figure 3*b* shows pressure contours (relative to the maximum pressure) in the muscle belly. The pressure increases monotonically from the peripheral muscle fibres at both sides towards the muscle centre. The pressure gradient (dp/ds) along the upper sheet increases from the left peripheral muscle fibre, reaches a maximum, and decreases again to zero in the muscle centre, and becomes negative in the right muscle half (figure 3*f*, see also the varying widths between the pressure contours in figure 3*b*).

PHILOSOPHICAL TRANSACTIONS OF THE ROYAL SOCIETY B BIOLOGICAL SCIENCES
PHILOSOPHICAL TRANSACTIONS OF THE ROYAL SOCIETY B BIOLOGICAL SCIENCES

Downloaded from rstb.royalsocietypublishing.org

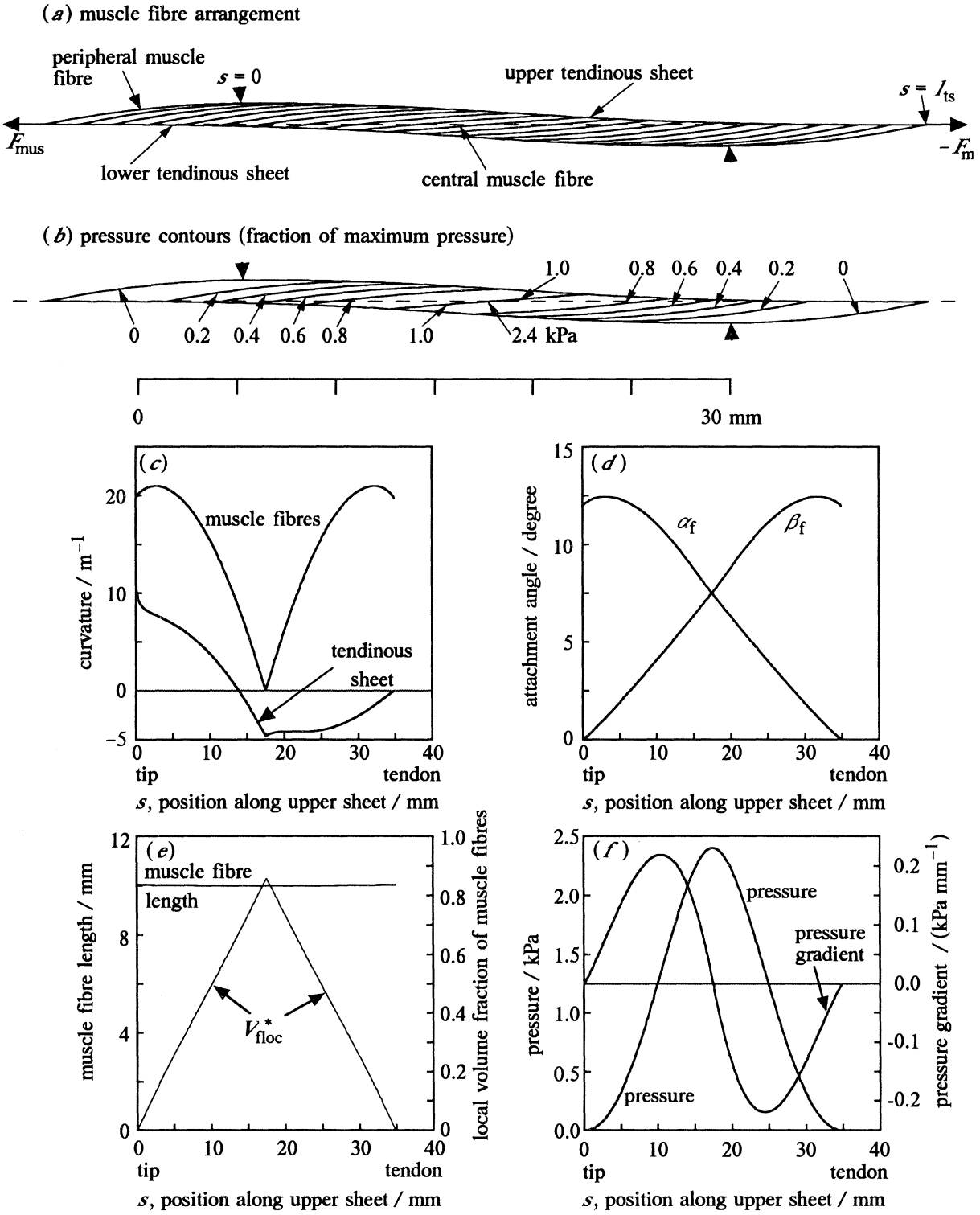

Figure 3. Illustration of the results of a simulation of a unipennate muscle architecture, with 600 muscle fibres used in numerical evaluation. Values of input and output parameters are given in table 1. (*a*) Muscle-fibre arrangement. At each side of the central muscle fibre, 10 fibres are shown, chosen at regular intervals along the upper (left side) and lower (right side) tendinous sheets. Arrow heads point to the transitions between tendinous sheet and peripheral muscle fibre. (*b*) Illustration of intramuscular pressure distribution in muscle belly. Contours show values of pressure in fractions of maximum pressure. The dashed line connects the tendons at both sides in (*a*) and (*b*). (*c*) Muscle-fibre curvature c_f and tendinous-sheet curvature c_s as a function of the position along the tendinous sheet s. (*d*) Attachment angles β_f and α_f as a function of s. (*e*) Actual and ideal (equation 13) muscle-fibre lengths as a function of s (the curves overlap completely, normal curves). Local volume fraction of muscle fibres V^*_{floc} as a function of s (thin curve). (*f*) Intramuscular pressure and pressure gradient dp/ds as a function of s. Further explanation is given in the text.

Downloaded from rstb.royalsocietypublishing.org

The absolute value of the pressure gradient is low near the peripheral muscle fibres because of the small attachment angles. Its low value at the muscle centre is caused by the small fibre curvatures (see also equation 2).

(*b*) *Unipennate simulations with large attachment angles of muscle fibres*

Figures 4*a*,*b* illustrate the fibre arrangement and normalized pressure contours for a simulation of a muscle belly with large attachment angles (parameter values in table 1). The central attachment angle was set to 15°, twice the value of figure 3. Other clamping conditions were chosen so as to generate tendinous-sheet lengths similar to those of figure 3. We do not show graphs for this muscle belly because they are of virtually identical shape as those of figure 3. Doubled amplitudes, however, occur compared with figures 3*c*,*d*, whereas the amplitudes of figure 3*f* are quadrupled. Compared with figure 3, the following differences should be noted:

1. On average, the tendinous-sheet curvatures are about doubled. The almost doubled central curvature (table 1) was needed to generate a tendinous sheet length of comparable magnitude to figure 3.
2. Muscle-fibre curvatures are about doubled along the peripheral tendinous sheets. By doubling both the fibre curvature and the fibre area, the pressure generated by the muscle fibres is about quadrupled (cf. equation 2). Of course, the pressure over the tendinous sheet (equation 3) should also be about quadrupled. The doubled attachment angles with the sheet lead also to an almost doubled tensile force T_s in the sheet (cf. equation 4). This leads, together with the doubled sheet curvature, to a quadrupled first term in equation (3). The second term was neglected and needs no further consideration. The third term is also about quadrupled by the doubled attachment angles. The maximum pressure in the muscle centre is about 9.54 kPa.
3. The length variation of the muscle fibres along the muscle belly is slightly larger, which corresponds to the stronger variation in α_f and β_f (cf. equation 13).
4. The calculated total volume fraction of the muscle fibres is only about 0.46 for this particular architecture, which is again unrealistically low (but see the discussion by Van Leeuwen & Spoor 1992). The local fibre fraction is similar to that of figure 3*e*.

Figure 4*c* shows the muscle-fibre arrangement for a simulation with equal input data as used in figures 4*a*,*b*, except that a value of 0.7 for parameter u (equation 14) was used instead of 1.1, while also a weaker negative central curvature of the tendinous sheets was applied so as to obtain similar sheet lengths. This leads, on average, to larger attachments angles along the sheet, resulting in a slightly higher maximum pressure (i.e. 10.47 kPa) in the muscle centre. It also leads to a different shape of the tendinous sheets, which now have two regions of negative curvature (concave outward), with a positive region in-between (figure 4*e*). Note again the slightly negative curvature of the sheet next to the tendon.

Figure 4*d* shows the muscle-fibre arrangement for a simulation with equal input data as used in figure 4*c*, except that a stronger negative central curvature of the tendinous sheets was chosen so as to obtain much shorter sheet lengths. This results in a lower maximum pressure (i.e. 7.57 kPa) in the muscle centre. The tendinous sheets have now a negative curvature over their whole length (figure 4*f*). The curvature of the sheet drops sharply towards the connection to the tendon. Close to the tendon, the third term in equation (8) is rather large because the attachment angle is quite large, while, at the same time, the interfibre space is less than for the other muscle bellies (i.e. η is relatively large; about half way along the fibres, most interfibre space is found between the superficial muscle fibres, see double arrow heads in figure 4*d*). Therefore, a rather strong compensation of the third pressure term is needed by the first term, which requires a rather strong negative curvature of the sheet close to the tendon.

The above comparison illustrates the prediction by Van Leeuwen & Spoor (1992) that the intramuscular pressure depends strongly on the architecture of the muscle. As explained by Van Leeuwen & Spoor (1992), the intramuscular pressure and force equilibrium are size independent (if the shape is constant), so that the muscle bellies of figures 3 and 4 can be enlarged or reduced to almost any particular size without an effect on the internal pressure.

(*c*) *Medial gastrocnemius muscle of the cat*

In the fixed specimens, the muscle-fibre bundles in the central region of the medial gastrocnemius of the cat were slightly, but unequivocally, S-shaped. This is in contrast to our assumption of a straight fibre in the central region. Most likely, the fixatives stiffen the endo- and perimysium so that relatively more force is transmitted perpendicular to the longitudinal direction of the muscle fibres. The altered force transmission may be an important cause of the S-shape. This viewpoint is supported by the rigor-mortis preparations, where this phenomenon was virtually absent. Therefore, rigor muscles were used for our comparison between muscle and model.

Figure 5*a* shows a drawing of the muscle-fibre arrangement in the central longitudinal plane of the medial gastrocnemius of the cat. The muscle was under tension and in rigor mortis before it was frozen and sectioned. The tendons at both ends are almost in line. A small deviation is understood from the partially muscular attachment at the femur. Only a small fraction of the muscle fibres run exactly in the exposed plane. Most of the drawn fibre directions are therefore composed of several parts of muscle fibres.

Figure 5*b* shows the fibre arrangement of a simulated muscle belly which is based on the distal half of the medial gastrocnemius (parameter values are given in table 1). The parameters were adjusted by hand until a satisfactory resemblance was obtained between muscle section and simulation. It would be unwise to

PHILOSOPHICAL TRANSACTIONS OF THE ROYAL SOCIETY B BIOLOGICAL SCIENCES
PHILOSOPHICAL TRANSACTIONS OF THE ROYAL SOCIETY B BIOLOGICAL SCIENCES

Downloaded from rstb.royalsocietypublishing.org

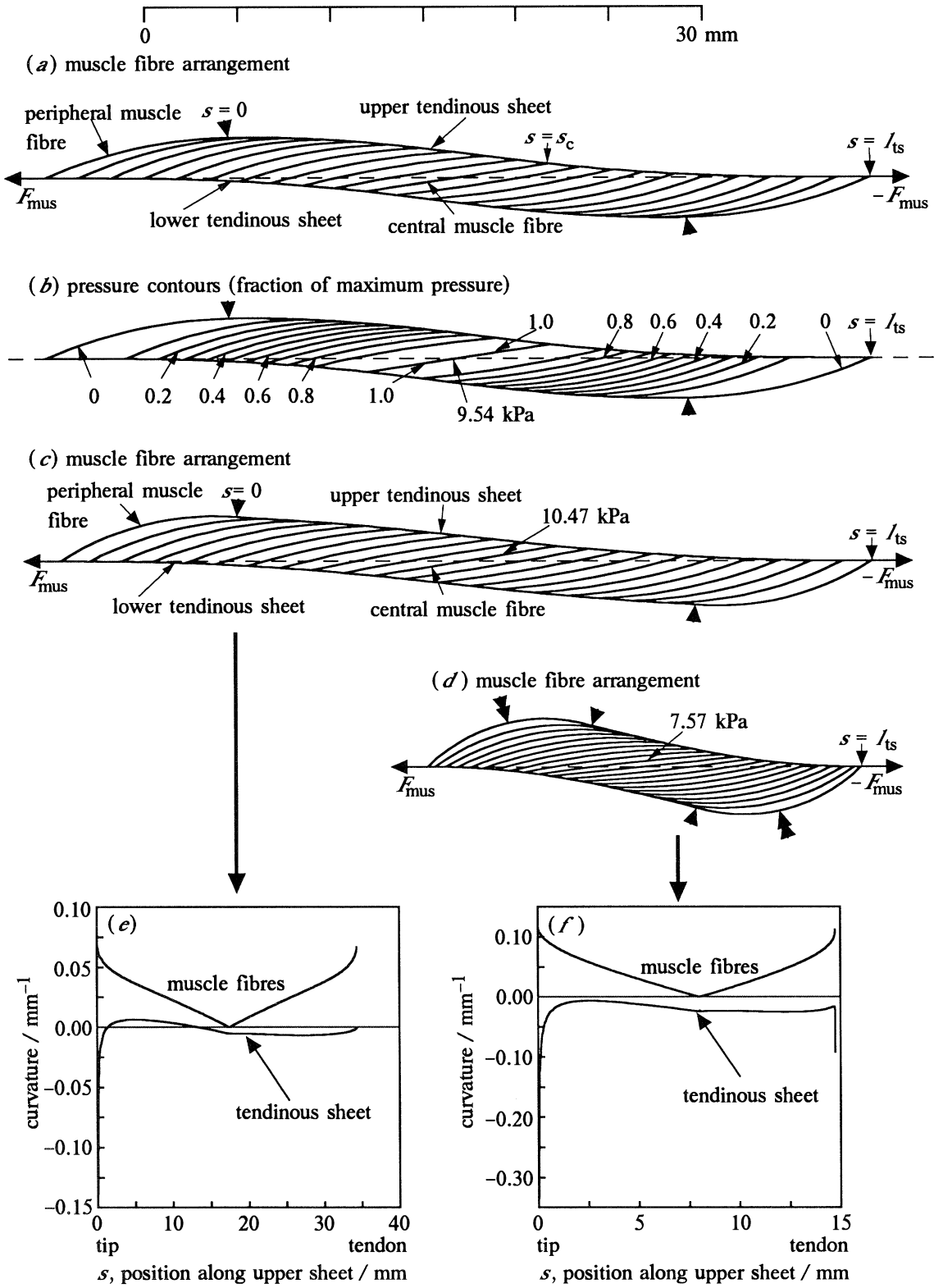

Figure 4. Illustration of the results of simulations of unipennate muscle architectures with larger attachment angles than in figure 3 (for values of input and output parameters see table 1), leading to more highly pennated muscle bellies. (*a*) Fibre arrangement in belly similar to figure 3, but with doubled attachment angle. (*b*) The same belly as in (*a*), but now with normalized pressure contours. (*c*) Fibre arrangement of simulation similar to (*a*), but with a value of 0.7 for exponent u in equation (14), resulting in quite dramatic changes in the tendinous sheet curvature (see plot *e*); two regions with negative curvature and a positive region in-between are now present. (*d*) Fibre arrangement similar to (*c*), but with a much shorter muscle belly. Now, the tendinous sheet is negatively curved along its whole length (see plot *f*). Double arrow heads point to position of maximum spacing between superficial fibres. See text for further explanation.

Downloaded from rstb.royalsocietypublishing.org

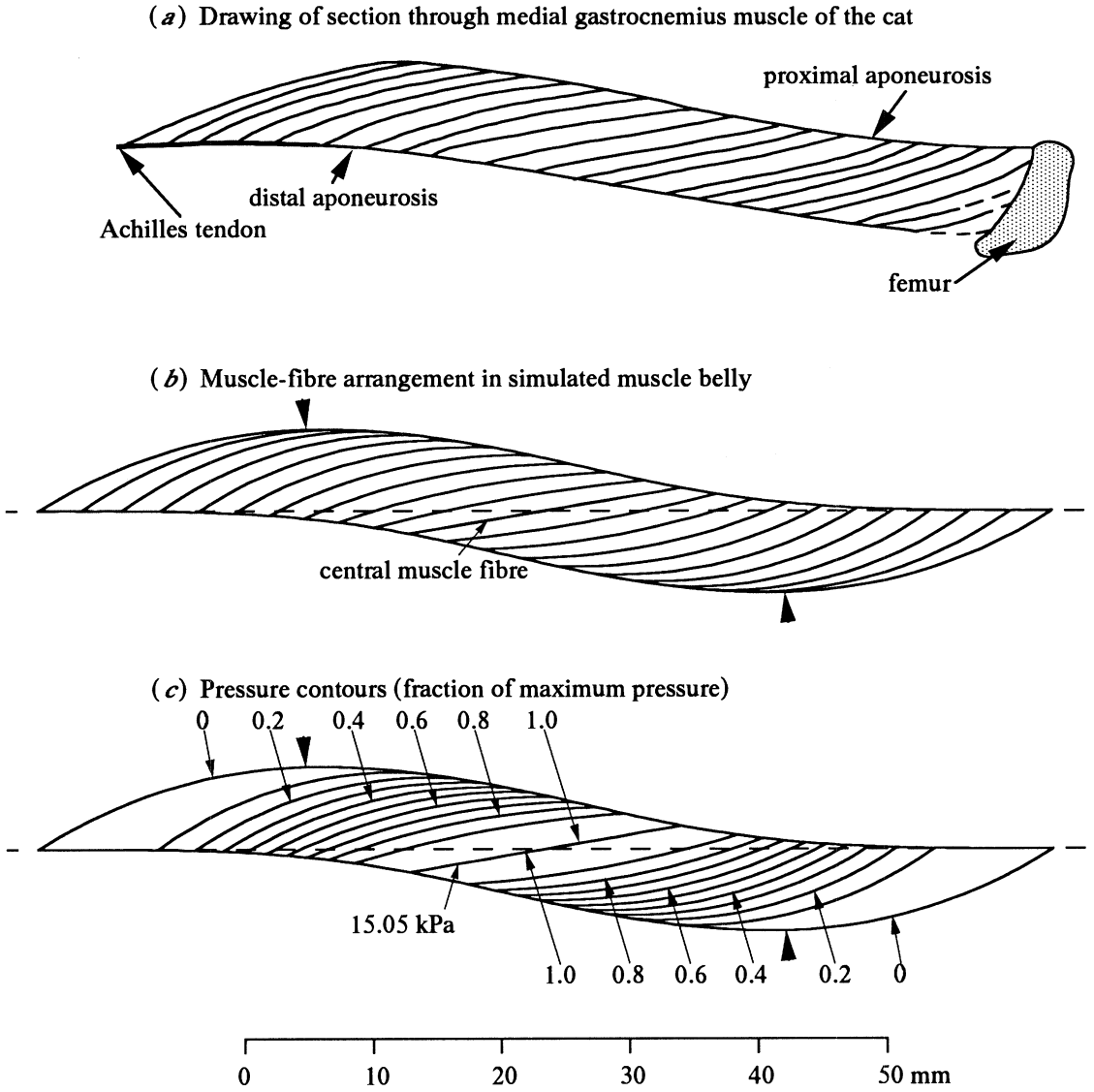

Figure 5. Comparison between the medial gastrocnemius muscle of the cat and a simulation. (*a*) Traces of the muscle-fibre directions and the shapes of the aponeuroses in the main longitudinal plane from a picture of a rigor-mortis muscle. The muscle was put under tension before it was frozen and sectioned. (*b*) Simulation of the muscle-fibre arrangement resembling that of the distal (left) half of (*a*). (*c*) Intramuscular pressure contours as a fraction of the maximum pressure (15.05 kPa) of the same simulation. Arrow heads in (*b*) and (*c*) point to the transitions between tendinous sheets and peripheral muscle fibres. The values of the input and output parameters are given in table 1.

aim at a perfect agreement because we did not include the three-dimensional arrangement of the muscle fibres, and we ignored the transverse tensile stress in the tendinous sheets. The proximal simulated muscle half deviates rather strongly from the cat muscle owing to our left–right symmetry assumption, and the complex attachment in the cat.

Figure 5*c* shows the simulated pressure distribution, which looks rather similar to that of figure 4*b*. The pressure levels, however, are significantly higher with a maximum pressure of 15.05 kPa in the muscle centre (using again 200 kPa for the fibre stress). The higher pressures are mainly the consequence of the larger attachment angles of the muscle fibres. Petrovsky & Hendershot (1984) measured the pressure in the medial gastrocnemius of the cat. Unfortunately, they specified the location of the pressure transducer in the muscle only qualitatively. At full activation and under isometric conditions, they obtained a maximum pressure 'in the belly . . .' of about 23 kPa. This value is in remarkable agreement with our calculations. The fibre stress of 200 kPa is probably lower than the maximum attainable isometric stress. Stresses of up to 300 kPa seem the upper limit, which would result in an upper estimate of 22.5 kPa. At the same time, the measurements are likely to overestimate the real pressure because the presence of a transducer tends to increase the local pressure (Gregg & Eckstein 1941).

6. GENERAL DISCUSSION

(*a*) *Some determinants of muscle architecture*

Muscle architecture is at least influenced by: (i) the size and shape of neighbouring structures; (ii) minimum requirements for shortening and work output by

Downloaded from rstb.royalsocietypublishing.org

each of the muscle fibres; (iii) mechanical stability; and (iv) the requirement of a close packing of the muscle fibres.

An example of the first influence is the spherical eye in cichlid fish around which the m. adductor mandibulae (a jaw muscle) has to fit without unfavourable mechanical interactions (Otten 1981). The present model and that of Van Leeuwen & Spoor (1992) seem to be useful tools in an analysis of the required architectural features. Another example is the gastrocnemius muscle in man which curves around the underlying tibia and soleus muscle (Van Leeuwen & Spoor 1992).

The second and the third factor are essential elements of the present model. As discussed by Van Leeuwen & Spoor (1992), the fourth requirement cannot easily be combined with the second one in a two-dimensional analysis. This is demonstrated by the calculated volume fraction of the fibres, which was too low as compared to a real muscle. The muscle fibre curvatures and orientations, required for the demands of mechanical stability and pennation angle–length relationship (equation 13), do not allow a close enough fit of neighbouring muscle fibres. In a three-dimensional muscle-fibre arrangement, this problem can easily be solved by allowing neighbouring muscle fibres from both sides to penetrate into the spaces between the series of longitudinally arranged muscle fibres (see Van Leeuwen & Spoor 1992). To allow an optimal filling of the muscle belly with muscle fibres, tendinous sheets should converge in width from the free edge to their connection with the tendon (figure 1). This arrangement allows also a 'smooth' transition from tendinous sheet to tendon. The local volume fractions of the muscle fibres as shown in figure 3*e* give an indication of the required width of the lower sheet relative to the upper sheet (in a three-dimensional arrangement with an optimal filling of muscle fibres).

In predicting unipennate muscle shapes, we aimed to select the most important parameters, while (quantitatively) confining ourselves to a two-dimensional analysis. Nevertheless, we think that our approach has led to an increased understanding of the shapes of muscles. Future, more advanced models may illuminate the limitations of our present judgements.

(*b*) *Intramuscular pressure and blood flow*

In the present simulations, we calculated maximum intramuscular pressures (using a muscle-fibre stress of 200 kPa for all fibres) in the range of 2.4 to 15.0 kPa. These pressures are on average somewhat lower than the pressures calculated for bipennate muscle bellies of comparable lengths in a previous study (Van Leeuwen & Spoor 1992). In the bipennate muscles, pressure is built up along the whole tendinous sheet, whereas only half the length of the muscle belly is used for the unipennate case. Furthermore, the muscle-fibre curvatures were, on average, largest in the comparable bipennate bellies. Therefore, during sustained contractions, continuation of blood flow through the muscle belly seems to be somewhat less problematic for unipennate muscle than for bipennate muscles of comparable length, height and fibre curvatures. Nevertheless, maximum pressures are high enough to obstruct blood flow in sustained contractions (blood pressure is about 4.5 kPa at the entrance of the capillaries, e.g. Charm & Curland 1974).

The maxima of the presently calculated pressures are lower than the pressure found in a simulation of the unipennate m. gastrocnemius medialis of people (Van Leeuwen & Spoor 1992). The human gastrocnemius is curved as a whole, resulting in tendons which are not in line. Furthermore, pressure is built up along the whole length of the muscle belly, which is comparable with the situation in bipennate muscles. The presently calculated maximum pressures for bellies with in-line tendons are smaller than those recorded for unipennate gastrocnemius and soleus (which is also likely to build up pressure over most of its length) by Petrovsky & Hendershot (1984).

In the recording of force–length diagrams of the gastrocnemius in the rat, the distal tendon is usually attached to the transducer, while the muscle is pulled rather straight (e.g. Woittiez *et al.* 1984). Most likely, this treatment transforms this fairly curved muscle into a belly with in-line tendons. This may alter significantly the position and magnitude of the high pressure centre in the muscle. The influence on the force production of the changed geometry is not very clear, but may be quite small. Experiments comparing the *in situ* mechanics with the mechanics of the straightened muscle belly are needed to settle this issue.

7. CONCLUSIONS

1. By extending the approach of Van Leeuwen & Spoor (1992), mechanically stable unipennate muscle architectures with in-line tendons were calculated. The internal pressure distribution is calculated from curved muscle fibres and tendinous sheets under tension.

2. Four determinants for unipennate architectures were distinguished: (i) influences from neighbouring structures; (ii) mechanical stability; (iii) generation of roughly equal specific power output and relative length change of the muscle fibres; and (iv) a close packing of the muscle fibres in the muscle belly.

3. The curvature of the tendinous sheets in unipennate muscles can be quite variable along the sheet. Regions of negative (concave outer surface) and positive (convex outer surface) curvatures may be present along one sheet.

4. As previously stated for bipennate muscles, the maximum intramuscular pressure generated depends on shape characteristics like attachment angles of muscle fibres, but not on the size of the muscle. The highest pressures are predicted for muscles with long tendinous sheets, large attachment angles, and strongly curved fibres.

5. A good qualitative resemblance was obtained between the observed shape of the central longitudinal plane of the medial gastrocnemius muscle of the cat and a simulation (figure 5).

PHILOSOPHICAL TRANSACTIONS OF THE ROYAL SOCIETY B BIOLOGICAL SCIENCES
PHILOSOPHICAL TRANSACTIONS OF THE ROYAL SOCIETY B BIOLOGICAL SCIENCES

Downloaded from rstb.royalsocietypublishing.org

6. Intramuscular pressures can be high enough (up to 15.05 kPa in the simulation of the medial gastrocnemius muscle of the cat) to obstruct blood flow. With the present model, the amplitude and location of high-pressure centres in unipennate muscles can be predicted.

Professor R. McNeill Alexander, Professor I. A. Johnston, and Dr M. R. Drost are thanked for useful comments on a draft of this paper. We also thank Dr C. Hoffmann for usage of the hind legs of his experimental animals, and Mr J. M. Guldemond for technical assistance.

REFERENCES

Charm, S.E. & Kurland, G.S. 1974 *Blood flow and microcirculation*. New York: Wiley & Sons.

Gregg, D.E. & Eckstein, R.W. 1941 Measurements of intramyocardial pressure. *Am. J. Physiol.* **132**, 781–790.

Huijing, P.A. & Woittiez, R.D. 1984 The effect of architecture on skeletal muscle performance: A simple planimetric model. *Neth. J. Zool.* **34**, 21–32.

Otten, E. 1981 Vision during growth of a generalized *Haplochromis* species: *H. elegans* Trewavas 1933 (Pisces, Cichlidae). *Neth. J. Zool.* **31**, 650–700.

Otten, E. 1985 Some numerical reflections upon a simple planimetric muscle model of Huijing and Woittiez. *Neth. J. Zool.* **35**, 517–520.

Otten, E. 1988 Concepts and models of functional architecture in skeletal muscle. In *Exercise Sport Sci. Rev.*, vol. 16 (ed. K. B. Pandolf), pp. 89–139. New York: MacMillan.

Petrovsky, J.S. & Hendershot, D.M. 1984 The interrelationship between blood pressure, intramuscular pressure, and isometric endurance in fast and slow twitch skeletal muscle in the cat. *Eur. J. appl. Physiol.* **53**, 106–111.

Spoor, C.W., Van Leeuwen, J.L., Van der Meulen, W.J.T.M. & Huson, A. 1991 Active force-length relationship of human lower leg muscles estimated from morphological data: a comparison of geometric muscle models. *Eur. J. Morph.* **29**, 137–160.

Van Leeuwen, J.L. 1992 Muscle function in locomotion. In *Mechanics of animal locomotion* (ed. R. McN. Alexander), pp. 191–250, Heidelberg: Springer-Verlag.

Van Leeuwen, J.L. & Spoor, C.W. 1992 Modelling mechanically stable muscle architectures. *Phil. Trans. R. Soc. Lond.* B. **336**, 275–292.

Wickiewicz, T.L., Roy, R.R., Powel, P.L. & Edgerton, V.R. 1983 Muscle architecture of the human lower limb. *Clin. Orthop. Rel. Res.* **179**, 275–283.

Woittiez, R.D., Huijing, P.A., Boom, H.B.K. & Rozendal, R.H. 1984 A three-dimensional model: A quantified relation between form and function of skeletal muscles. *J. Morphol.* **182**, 95–113.

Zajac, F.E. 1989 Muscle and tendon: properties, models, scaling, and application to biomechanics and motor control. In *CRC critical reviews in biomedical engineering* (ed. J. R. Bourne), vol 17, pp. 359–411. Baco Raton: CRC Press.

Received 8 March 1993; accepted 24 May 1993

PHILOSOPHICAL TRANSACTIONS OF THE ROYAL SOCIETY B BIOLOGICAL SCIENCES

PHILOSOPHICAL TRANSACTIONS OF THE ROYAL SOCIETY B BIOLOGICAL SCIENCES